Effects of polymer adsorption on the effective viscosity in microchannel flows: phenomenological slip layer model from molecular simulations

Teresa Lynne Palmer[a,b,c,*], Thomas Asadi Espås[c,d], Roar Skartlien[c,e]

[a] *University of Stavanger, P.O. Box 8600, N-4036 Stavanger, Norway*
[b] *IOR Centre of Norway*
[c] *Institute for Energy Technology, P.O. Box 40, N-2027 Kjeller, Norway*
[d] *University of Manchester, Oxford Rd, Manchester, M13 9PL, UK*
[e] *Norwegian University of Science and Technology, Ugelstad Lab., NTNU, N-7491 Trondheim, Norway*

Abstract

Molecular simulations (Dissipative Particle Dynamics - DPD) were used to quantify the effect of polymer adsorption on the effective shear viscosity of a semi-dilute polymer solution in microchannel Poseuille flow. It is well known that polymer depletion layers develop adjacent to solid walls due to hydrodynamic forces, causing an apparent wall slip and reduced effective viscosity (increased total flow rate). We found that depletion layers also developed in the presence of hydrodynamically rough adsorbed layers on the wall. Polymer-polymer (steric) repulsion between flowing and adsorbed polymer expanded the depletion layer compared to no-adsorption cases, and the effective viscosity was reduced further. Desorption occurred for higher shear rates, reducing the repulsion effect and shrinking the depletion layers. A phenomenological algebraic model for the depletion layer thickness, including a shear modified adsorption isotherm, was developed based on the simulation data. The depletion layer model can be used together with the effective viscosity model we developed earlier.

Keywords: polymer migration, polymer adsorption, polymer rheology, DPD molecular simulation

*Tel.: +47 63 80 64 67; Fax: +47 63 81 11 68
Email address: tlpalmer@yahoo.com (Teresa Lynne Palmer)

1. Introduction

A laminar flow of a polymer solution exhibits wall-normal migration of polymer with lowered polymer concentration near the walls [1, 2, 3, 4, 5]. This "depleted" volume has lower viscosity than the bulk flow, thereby acting as a lubricating layer that increases the volumetric flux of liquid for the same pressure gradient[5]. The flow and adsorption behavior of polymer is of fundamental importance in many applications, from chromatic separation, protein adsorption, and polymer flooding in enhanced oil recovery. The reduction of effective viscosity is an important aspect to consider in the field of polymer flooding [6], since the channel width or pore diameter is on the order of microns and the depleted volume fraction can therefore be significant. A reduction of the effective viscosity by a factor of at least two is found for HPAM (partially hydrolyzed polyacrylamide) solutions in plane-wall channels when the channel width is reduced from ten to one micron [5]. It is well established that migration and depletion is a fundamental mechanism that is likely to occur also in the complex geometry of oil reservoir rocks through experimental evidence obtained with core flooding [6, 7, 8].

If there is no adsorption, the depletion layer expands with shear rate for Weissenberg numbers above unity and the shear thinning effect is amplified. Wall-normal migration away from clean walls occurs primarily due to hydrodynamic viscous Stokes-flow interaction with the walls. The associated drift-flux is balanced by a diffusion flux back towards the walls [2, 9] and the equilibrium state has lowered polymer concentration close to the walls, and higher concentration in the core of the channel. A combined algebraic effective viscosity and depletion layer model was developed by us [10] for the case of no adsorption. This phenomenological model was based on DPD (Dissipative Particle Dynamics) simulations of polymer chains in water, and the hydrodynamic theory of Ma and Graham for dumbbells[2].

The focus of the current paper is primarily to study the behavior of the depletion layer in the presence of adsorbed polymer on the channel walls. The adsorbed layer may affect the depletion layer thickness by polymer-polymer interaction, and possibly by increased wall roughness. In polymer flooding with high molecular weight HPAM, we expect flexible polymer chains that are weakly attached to the surface. The resulting polymer layers are diffuse with a relatively small fraction of the polymer segments attached to the surface with unattached segments extending into the flow in the form of loops or free ends [11]. The adsorbed density is influenced by the ionic components

of the solvent and the chemical composition of the given mineral [12, 13]. Although HPAM is designed to reduce adsorption, some polymer adsorption will occur depending on the mineral composition, and cause permeability reduction [6, 8]. At low salinity (low ion contents in the solvent), repulsion between HPAM polymers occurs due to the electrostatic forces between the carboxylate groups. This may limit the adsorbed surface density, but also provide a repulsive force between polymers in solution and adsorbed polymer, thereby expanding the depletion layer.

Theories for polymer adsorption without flow predict "Langmuir-like" isotherms with an initial steep rise of the surface density, followed by a nearly horizontal semi-plateau, as a function of bulk concentration [14]. However, experimental isotherms usually show a gradual increase, while a well-defined plateau is not always observed [14]. Furthermore, when diluting the solvent, the desorbed amount is often very small, suggesting that polymer adsorption may appear to be irreversible in some cases. The likely reason for this is due to the multiple contacts each chain makes with the surface, and a small probability of simultaneous disengagement of these contact points [11].

It is unlikely that Langmuir isotherms hold for polymer flooding, primarily because the shear will affect the adsorption and desorption kinetics. In general, the surface density is reduced with increasing shear rate [15]. Flow-induced desorption of polymer occurs with sufficiently large shear stresses and is more efficient for larger molecular weight[11]. Polymer chains in solution orient with the flow and even moderate shear rates are able to inhibit the cross-flow diffusive transport towards the surface, and this adsorption inhibition is also more efficient for larger molecular weight. It is therefore likely that the adsorbed density in a steady-state equilibrium situation is dependent on the pre-adsorbed state of the surface before the shear stresses are applied. This history effect is of consequence for polymer flooding, in the sense that the surface density during a secondary injection may not desorb to the level of the first primary injection.

We studied how the depletion layer thickness, adsorbed wall density and effective viscosity responded to varying shear rates by using DPD (Dissipative Particle Dynamics) simulations. The simulation data were then used in conjunction with a modified Ma-Graham model for the wall-to-wall polymer concentration profile, to construct a first-order phenomenological model for the depletion layer thickness as function of Weissenberg number or normalized shear rate. This can further be used in effective viscosity models of the type we developed earlier [10].

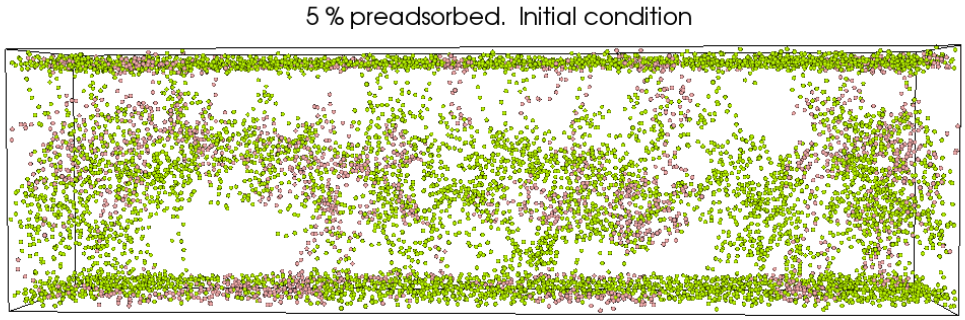

Figure 1: Adsorption equilibrium for the preadsorbed case, before shear is applied. The walls (top, bottom) are partially covered with a monolayer of polymer. The apparent voids in the bulk volume is due to polymer being adsorbed earlier, leaving temporary voids. Some polymers are marked in pink, and the water is not shown.

2. DPD setup with adsorption

A detailed description of DPD molecular simulations can be found in the now extensive literature [16, 17, 18, 19, 20, 21]. DPD preserves the viscoelastic and shear thinning rheologies of the polymer solution, as well as the characteristic adsorption isotherm properties. Polymers are modelled as long chains of DPD particles (beads), where bead pairs are linked by a "spring-force", giving rise to fluid visco-elasticity by viscous coupling to the solvent. The interaction between the polymer chains and the solvent (here, water) depends on the polymer deformation, stretching and alignment with the flow, and as a result the polymer solution is both shear thinning in shear flow, and elastic in extensional flow. The current study delas only with Poseuille shear flow. It is essential to have high Schmidt numbers ($Sc \gg 1$) to achieve realistic polymer migration effects [22, 23, 24], and the DPD parameters were adjusted to achieve $Sc = 600$ as described earlier[10]. The viscous hydrodynamic coupling to the confining walls is automatically accounted for via the molecular forces. The adsorption isotherm (by physisorption) and polymer solubility (in the solvent fluid) can be controlled by the strengths of the molecular interaction potentials that are input to the model.

A 3D DPD simulator for parallel processing was tailored to oil/water/polymer flow in microchannels with arbitrary wall geometries[10]. Our code was parallelized using a domain-decomposition method with a parallel linked cell-list approach, which was first introduced for MD simulations [25] and later generalized to DPD [26].

2.1. Wall velocity boundary conditions

A body force G was applied to all DPD beads (both water and polymer) to pull the fluid through the channel. It is essential to have no-slip boundary conditions at the walls, otherwise the effective viscosity will be artificially lowered due to water beads slipping along the wall. To obtain no slip conditions in general, the fluid beads that come close to the wall are assigned a zero-mean velocity. The random velocity components were drawn from a Maxwell-Boltzmann distribution at the kinetic temperature of the system [27, 28]. This approach was generalized by us for any non-flat wall geometry [10]. The wall structure was modelled with randomly placed beads within a well defined mathematical and smooth surface (here, a flat plane).

2.2. Interaction parameters

The conservative DPD forces were controlled via the DPD parameter matrix

$$a_{ij} = \begin{pmatrix} & w & p & s \\ w & 25 & 50 & 25 \\ p & .. & 100 & 50/0 \\ s & .. & .. & .. \end{pmatrix}, \tag{1}$$

where w, p, s, stand for water, polymer, and wall (substrate) beads, respectively. Higher positive value means larger repulsion force between the beads. The force potentials $a_{ij}U(r)$ vary quadratically with bead distance r, generating a linearly decaying force with increasing distance. The interaction parameters represent a scaling of the magnitude of the same quadratic potential U. The $a_{ww} = 25$ parameter is the water - water coupling, chosen to match the compressibility of water [16]. For the polymer to be soluble in water, $a_{pp} > a_{wp}$, which provides extended polymer chains. The other parameters also influence the solubility properties to some degree, but also the magnitude of the viscosity of the solution [10].

Adsorption on the wall can be controlled by choosing appropriate wall-polymer interaction parameters that reproduce the desired isotherm for zero velocity conditions. A reduced polymer-wall parameter a_{ps} increases the adsorbed density. We used values of $a_{ps} = 0$ with adsorption, and $a_{ps} = 50$ without adsorption. A reasonable amount of adsorbed polymer was obtained, without completely depleting the core volume of the channel.

The wall bead density was chosen to be 4 times larger than water density to prevent the water beads from diffusing into the partially porous wall

structure. The matrix given above is corrected for this density enchancement to achieve the same force magnitude (the wall-related parameters are divided by 4 in the code when the wall density is increased by the same factor).

2.3. Initial conditions for primary and secondary polymer injection

Two different initial conditions were used, with regards to the adsorbed layer. For *Set 1 (primary injection)* we inserted a uniform volume fraction of 5% and 10% polymer throughout the channel, and let the polymers adsorb on the clean wall after the body force was applied. This scenario is similar to primary injection into a reservoir subject to adsorption inhibition by polymer stretching in the shear field.

For *Set 2 (secondary injection)* we let the polymers adsorb to the wall before the body force was applied, and thermodynamic equilibrium between the bulk and adsorbed densities was reached (Figure 1). Then, we applied the body force. This approach is similar to a secondary injection into a reservoir where the adsorbed layer is already present before the shear is applied. The case was set up to that the bulk volume fraction in equilibrium was close to 5% throughout the channel also in this case.

For (*Set 3 - no adsorption*), we run a few reference cases at varying shear rates without adsorption, and the bulk volume fraction was 5% also in these cases. These cases were run to in order to assess the difference in the depletion layer and effective viscosity with and without polymer adsorption.

The volume of the simulation domain is necessarily limited, and it is currently not computationally possible handle large enough domains to encompass the full length of a typical HPAM polymer. However, an essential quantity that can be matched is the total length of polymer chain per volume of water (shorter chains, but a larger number of them),

$$l_v = \frac{\rho_p L_p}{m_p}. \tag{2}$$

This results in a realistic contact area between the polymers and the water per volume unit, and hence the stress coupling between the water and the polymers should be of correct magnitude. The polymer relaxation timescale λ will however be shorter, resulting in lower Weissenberg number $Wi = \lambda\dot{\gamma}$ for a given shear rate $\dot{\gamma}$. By assuming non-degraded HPAM molecules of mass $m_p = 4 \times 10^6\ Da$, the polymer length is about $L_p = 10\ \mu m$ [29]. For a polymer mass density in solution of $\rho_p = 1000\ ppm = 10^{-3} gm/cm^3$,

we obtain a volume fraction of polymer beads in the DPD simulations of $\phi_p = 5\%$, when the equilibrium bead separation is comparable to the DPD length unit of $r_c = 0.64 \times 10^{-9}$m. Polymers of bead length up to $N = 120$ were tested in our previous work [10] and we found essentially the same behavior as for $N = 60$.

2.4. Effective viscosity evaluation and domain size

The simulations were set up for Poseuille flow between flat walls. The effective viscosity was evaluated according to its definition in terms of the ratio between the pressure gradient (here, applied force G) and total flow rate U over the channel cross section h,

$$\mu_e = \frac{h^2}{12}\frac{G}{U}. \tag{3}$$

The effective viscosity was evaluated as function of channel width h the channel-averaged Weissenberg number

$$Wi = \langle\dot{\gamma}\rangle\lambda, \tag{4}$$

where the average shear rate is

$$\langle\dot{\gamma}\rangle = \frac{1}{h/2}\int_{-h/2}^{0} \partial_y u(y)dy = \frac{u(0)}{h/2}. \tag{5}$$

The polymer relaxation time λ is fixed and determined by the DPD parameters[10].

To determine the effective viscosity, the velocity profile $u(y)$ was integrated over the full channel width to obtain the average velocity U. We started the simulations with the polymers randomly distributed in the water. The body force G accelerated the fluid up to a steady flow, with stable velocity and concentration profiles with depleted layers. Time averaging was then performed over the water and polymer bead velocities to evaluate U.

We used channel widths in the range $h \in [6, 40]$ nm, but most of the data is for a relatively narrow $h = 13$ nm, so as to have a significant depletion layer effect on the effective viscosity. This corresponds to 20 DPD units (of $r_c = 0.64 \times 10^{-9}m$). The spanwise (crossflow) dimension was also 20 DPD units. The boundary conditions were periodic in the spanwise and flow-aligned directions. The length of the domain size in the flow-aligned direction was 80 DPD units for a polymer of chain length $N = 60$ to avoid wrap-around effects.

Figure 2: Flow visualization for the preadsorbed case, in steady state after shear is applied. The adsorbed layers and the depletion layers (voids) between the core flow and the adsorbed layers are clearly visible. The walls (top, bottom) are partially covered with a monolayer of polymer. Some polymers are marked in pink, and the water is not shown. The flowing polymers are stretched out and align with the flow.

3. Results

3.1. Qualitative description

Set 1 were executed with no polymer on the walls initially, with 5 % and 10% polymer solutions in the bulk. This initial condition is a non-equilibrium situation between the surface and the bulk. After a transient phase of adsorption, the simulations were run long enough to come to an equilibrium in steady flow. For comparison, *Set 2* was run with preadsorbed polymer onto the walls initially, and had 5 % polymer solution in the bulk. After shear was applied, some of the polymer desorbed by the shear forces before a new equilibrium state was reached. A visualization for the preadsorbed case in equilibrium is shown in figure 2. A layer of polymer remained on the wall, and a depletion layer developed between the adsorbed polymers and the bulk flow. The polymer chains stretched out and aligned with the direction of the flow, indicating a flow regime with shear thinning. *Set 1* showed similar behavior with adsorbed layer, depletion layer, and core region with flowing polymer. One can conclude that depletion layers also form in the presence of more hydrodynamically rough adsorbed layers.

The velocity profile for the 5% case *(Set 1)* without preadsorption is shown in figure 3. The velocity profile was obtained after adsorbtion equilibrium was reached. The velocity goes to zero at the wall since there is no slip at the wall. Close inspection shows that the velocity (averaged over both water and polymer beads) is slightly reduced inside the adsorbed layer compared to the no-adsorption case. For the preadsorbed case with the highest surface

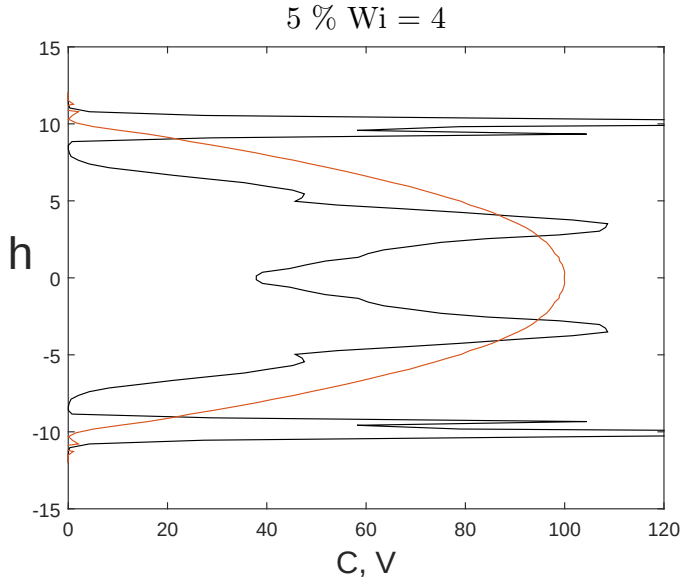

Figure 3: Velocity and concentration profiles for the 5% case *(Set 1)* at $Wi = 4$. The height scale is normalized to the DPD unit length, and the wall is at $\pm$ 10 DPD units. The concentration unit is counts per bin. The velocity is scaled to fit the plotting range.

density (80% surface coverage for the higher Wi), the velocity was reduced only by about 30% in the adsorbed layer, indicating that the polymers moved substantially while being adsorbed to the wall (sliding along the wall).

The concentration profile in figure 3 shows the characteristic "volcano" shape in the core flow, and the two outer concentration peaks correspond to the adsorbed layers. The depleted region corresponds to the local concentration minima (near zero concentration in the figure) close to the adsorbed layers. The density gradient from the core flow towards the depleted layers are in general smoother than the gradient at the boundary between the adsorbed and depleted layers.

3.2. Definition of the depletion layer width

The depletion layer thickness δ was defined as the distance from the wall where the polymer concentration c is equal to its half-value,

$$c(\delta) \equiv \frac{1}{2}\langle c(y)\rangle, \tag{6}$$

where averaging $\langle..\rangle$ was performed over the full volume of the channel, excluding the adsorbed layer. The polymer bead number density was measured

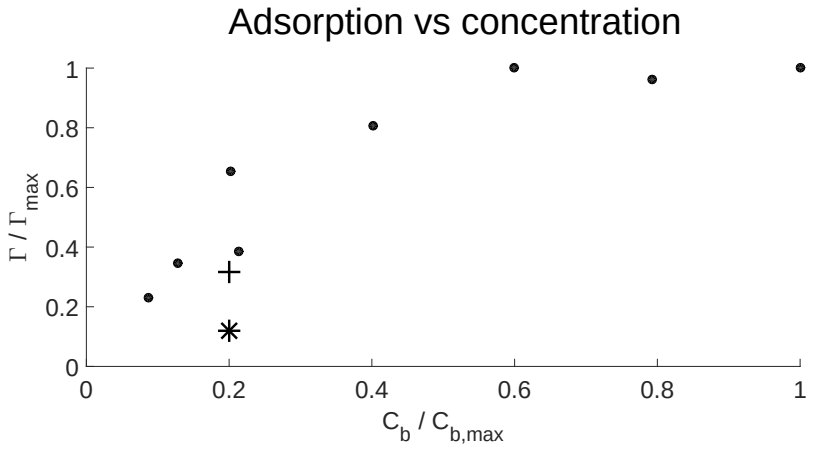

Figure 4: Adsorption isotherm for $Wi = 0$ (without flow) from the simulations (filled circles). The + and * symbols show the adsorbed density for Weissenberg number 4 and 8, respectively, for the 5% case without preadsorption. Lowered density is consistent with shear induced adsorption inhibition.

in suitable bins Δy in the wall normal direction y. The polymer concentration profile $c(y)$ could then be estimated [10]. It is reasonable to define the channel width in terms of the distance between the zero points in velocity, and to measure the depletion layer thickness relative to these points. For fully covered surfaces with strong surface-polymer interaction leading to essentially non-moving polymer, it would be more correct to use the outer boundary of the adsorbed layer as the reference point, and correct the channel width accordingly when estimating the effective viscosity.

3.3. Adsorption behavior

To test the ability of regenerating "Langmuir-like" isotherms, we measured the adsorbed density with no flow and a number of different bulk concentrations. A volume visualization is shown in Figure 1 of the preadsorbed case (5% bulk volume fraction) before the body force was applied. The adsorbed layer was essentially a monolayer. Monolayer formation is also expected when the polymers repel each other. Otherwise, one could expect multilayer formation. By analyzing the time sequence, we found that the ap-

parent voids in the bulk volume were temporary and due to polymers being adsorbed at earlier times. We note that the polymers are indeed soluble in the water (given the interaction matrix a_{ij}) and do not leave voids due to phase separation.

The adsorption isotherm for a range of bulk concentrations is shown in Figure 4. It is consistent with a Langmuir isotherm where the surface density saturates above a certain bulk concentration $c \simeq 1/K$,

$$\Gamma = \Gamma_{max} \frac{Kc}{1 + Kc}, \tag{7}$$

where Γ is the measured excess surface density, Γ_{max} the saturated surface density, K is the equilibrium constant for the bulk-surface exchange, and c is the bulk concentration of polymer.

The adsorbed density for the 5% solution with flow (initially clean surface) is also plotted Figure 4 for $Wi = 4$ and $Wi = 8$, showing that the surface density is reduced considerably with shear. Shear inhibits the adsorption for these cases due to polymer stretching and deformation that reduces cross channel diffusivity[11]. The other effects that inhibit adsorption is the hydrodynamic repulsion force that is the origin of the depletion layer[2], and repulsion to adsorbed polymer.

The adsorbed polymer chains stretched out and oriented with the flow, and large parts of the chains appeared to be adsorbed on the wall, with short loops extending into the flow. Polymer with only one end attached to the surface were rarely observed, as it would be a transient phenomenon. The concentration peaks at the wall (Figure 3), appear to be wider than the polymer radius. The reason for this is that short segments of the polymers extend into the flow, and the wall itself is rough with small gaps where the polymer can adsorb.

The amount of polymer adsorbed onto the walls as function of Weissenberg number is shown in the right panel of Figure 6 for all cases. By comparing the 5% and 10% cases, it is evident that higher concentration leads to more adsorbed polymer, as one would expect from any isotherm. However, the amount of adsorbed polymer is reduced with increasing shear rate due to inhibited adsorption for these cases. The pre-adsorbed case, corresponding to secondary polymer flooding into a channel, is shown in figure 6 with the label "5%+". The simulations begin with the walls fully covered. As the Weissenberg number increases, the shear stresses on the polymer layer increases, and some of the polymers desorb from the wall.

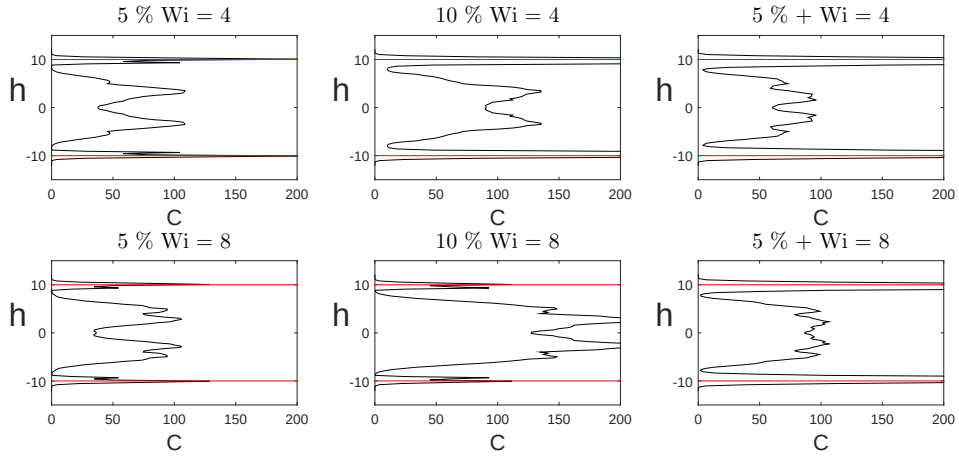

Figure 5: Concentration profiles for 5% (left), 10% (center) with initially clean walls, and the 5 %+ preadsorbed case is shown to the right. The height scale is normalized in terms of the DPD unit length, and the concentration is in terms of counts per bin.

The total number of polymer chains for the 5% preadsorbed run and the 10% run are the same. This is interesting because in a non-flowing situation, the two cases would have identical adsorbed densities and identical bulk densities. The adsorbed densities are dramatically different with shear, the higher density for the desorption case (5%+ preadsorbed), consistent with the literature [11].

3.4. Concentration profiles

Concentration profiles for $h = 13$ nm for different Weissenberg numbers are shown in Figure 5. The thickness of the adsorbed layer (in terms of the width of the concentration peaks) does not vary much with Wi due to monolayer adsorption, and corresponds to the polymer chain radius including the undulations of the adsorbed polymer. However, the fraction of surface covered varies with bulk polymer concentration and shear rate, so that the amplitude of the concentration profile changes accordingly.

The figure also confirms that the bulk concentration is larger with higher shear as the surface density is lowered. This is very clear for the 10% case, where adsorption inhibition is at work. For the preadsorbed case (5%+), the difference between high and low shear rates is small due to the relatively inefficient desorption by the shear forces.

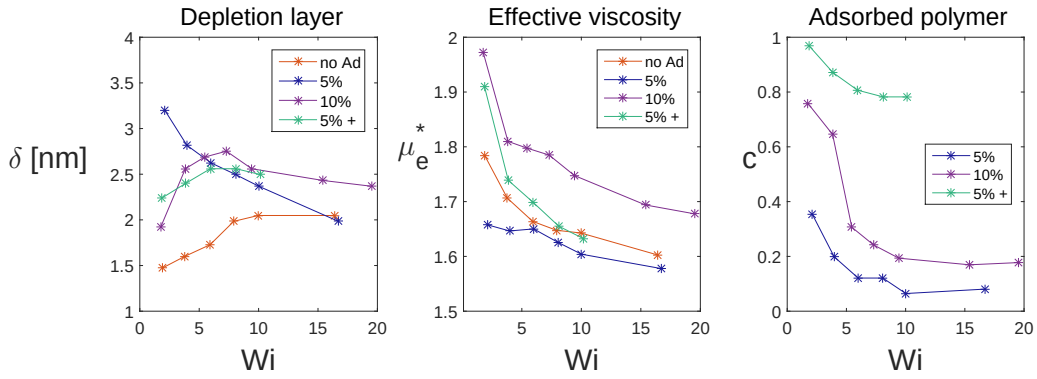

Figure 6: Depletion layer and effective viscosity versus Weissenberg number, with and without adsorption. The preadsorbed case is marked with 5%+. The channel width is here $h = 13$ nm. The area fraction covered by polymer is given in the right hand panel.

3.5. Depletion layer thickness as function of shear rate

Figure 6 shows the depletion layer thickness as a function of Weissenberg number (left panel). In our earlier work without adsorption[10], we found an approximately linear increase with Weissenberg number up to a constant asymptotic value for high Wi. This is also confirmed with the new simulations (Figure 6, left panel with label "no Ad"). With adsorption, it is evident that the depletion width can in fact *decrease* for increasing Wi. The reason for this behavior is most likely the repulsive force between the polymers in the bulk and adsorbed polymer, since the repulsion force on a bulk polymer decreases with decreasing adsorbed density. There is also an apparent convergence between non-adsorbing and adsorbing depletion layer thicknesses for very high Wi, and this is consistent with desorption and smaller repulsion effect for higher Weissenberg number.

For any given Weissenberg number, there is no clear correlation between the adsorbed density of polymer (Figure 6, right panel) and the depletion layer thickness (left panel). This is contrary to expectation if the main effect is polymer repulsion with respect to the adsorbed layer. In section 4, we analyze this further and find that the most likely explanation is a delicate balance between the repulsion effect that expands the depletion layer and gradient diffusion back towards the wall that shrinks the depletion layer. The latter depends on the density gradient at the boundary of the depletion layer, but also the density itself when non-dilute polymer-polymer interaction in the bulk is important.

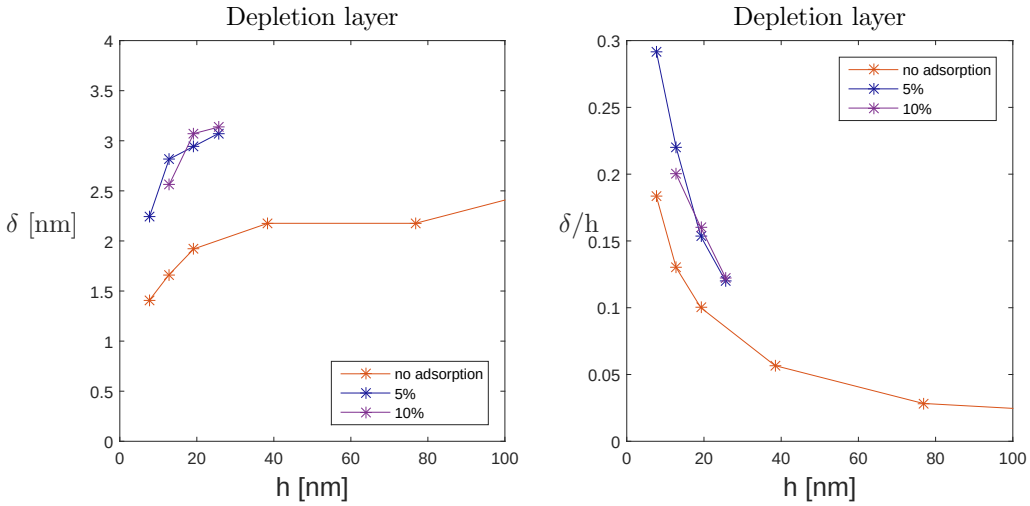

Figure 7: Depletion layer as function of channel width for $Wi = 4$, without preadsorption.

3.6. Effective viscosity

All the runs show reduced effective viscosity with higher Weissenberg number, which is consistent with shear thinning (Figure 6 middle panel). For a given Weissenberg number, the effective viscosity is lowered by an expansion of the depletion layer. In general, we also expect that the effective viscosity increases with increasing bulk concentration between the depletion layers. The two 5% cases had similar bulk concentrations in equilibrium (Figure 8, lower right panel). The reason for this is that the desorption for the preadsorbed 5% case is not very efficient, and the adsorption is small for the non-preadsorbed 5% case. Since these two cases have similar bulk polymer contributions to the effective viscosity, the difference in effective viscosity is mainly due to a difference in the depletion layer thickness for the same Weissenberg number. The depletion layer thickness is larger for the case with no pre-adsorbtion for $Wi < 5$ (by comparing the blue and red lines in the left panel in Figure 6) and the effective viscosity is therefore significantly lower (middle panel). The 10% case had similar depletion layer thickness as the preadsorbed case (violet and green, left panel), but much higher effective viscosity due to higher bulk concentration (Figure 8, lower left panel).

3.7. Depletion layer thickness as function of channel width

We also ran simulations with varying channel widths at $Wi = 4$ with 5% and 10% polymer solution without preadsorbtion. The results are shown in figure 7, and it is confirmed that the depletion layer width is larger with adsorption also for a range of channels widths from 10 to 30 nm. Furthermore, the depletion layer thickness increases monotonically as function of channel width, similar to the no-adsorption case. The right hand panel shows the depleted volume fraction δ/h, which is the main parameter for effective viscosity reduction. The effective viscosity is normally reduced when the depleted volume fraction increases for narrower channels. However, the increased bulk concentration may counteract this effect to some degree.

4. Phenomenological model for the depletion layer

In this section we develop an extended depletion layer thickness model based on the Ma and Graham concentration profile model for dumbbells and the simulation data. New mass flux terms are added that represent the repulsion between adsorbed polymer and polymer in solution, and enhanced gradient diffusion towards the walls for non-dilute solutions. The effective viscosity model we developed earlier [10] with input parameter δ/h, can be used in conjunction with the new model for δ.

4.1. Modified depletion layer model with adsorption

The cross-channel mass flux of non-interacting dumbbells in a dilute solution with no wall-adsorption is to leading order [2]

$$j = V_d(y)n - D\partial_y n, \tag{8}$$

where V_d is the local drift velocity due to Stokesian interaction between the dumbbell and the wall, n is the number density of dumbbells, and D is the Brownian diffusivity

$$D = \frac{kT}{12\pi\eta a}, \tag{9}$$

where a is the effective hydrodynamic radius of the dumbbell, and η is the solvent viscosity.

We introduce a drift velocity V_{pp} due to interaction between a polymer in the bulk and the adsorbed polymers, so that the new mass flux is

$$j = V_d(y)n - D\partial_y n + V_{pp}(y)n, \tag{10}$$

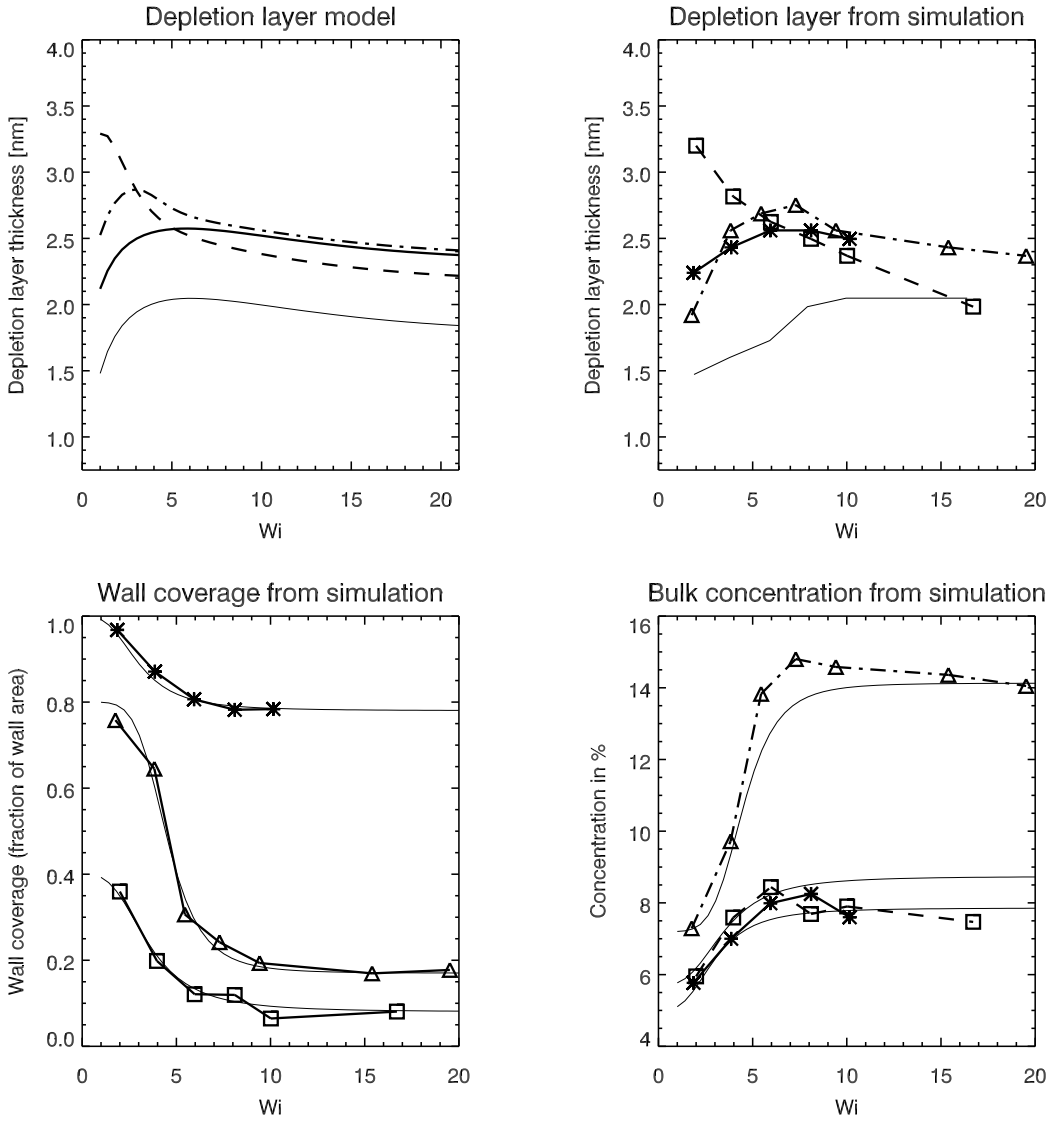

Figure 8: Depletion layer as function of Weissenberg number. *Upper panels:* Phenomenological model and simulation results for 5% polymer (dashed line and squares), 10% polymer (dash-dot line and triangles), and preadsorbed case with 5% polymer in the bulk (full line and asterisks). The thin line shows the case without adsorption (and 5% polymer in the bulk). *Lower panels:* Wall coverage in fraction of total surface area, and bulk volume concentration in percent as function of Weissenberg number. The symbols have the same meaning as for the upper panels. As the wall coverage decreases (and the bulk concentration increases), the depletion layer decreases mainly due to lowered wall repulsion.

with

$$V_{pp}(y < L/2) = +V_p[1 - H(y - y_p)], \quad (11)$$
$$V_{pp}(y > L/2) = -V_p H(y - (L/2 - y_p)). \quad (12)$$

This formulation accounts for the short range effect of the polymer-polymer repulsion near the wall. H is the Heaviside step function, y_p the effective maximum interaction distance between the dumbbell and the wall, and $V_p(Wi)$ varies only with the Weissenberg number to first order.

In Poseuille flow between two flat walls separated by a distance h, one can superpose the two single wall interactions as an approximation for the net drift velocity due to viscous Stokes interactions with the wall,

$$V_d(y) = \frac{K(y)}{y^2} - \frac{K(h-y)}{(h-y)^2}, \quad (13)$$

with a notable distance variation of $1/y^2$, and

$$K(y) = \frac{3}{64\pi\eta n}(N_1(y) - N_2(y)), \quad (14)$$

in terms of the normal stress difference $N_1 - N_2$ of the dumbbells [30]. In plane parallel flow, $N_1 = \tau^p_{xx}$ in terms of the polymer normal stress in the flow direction, and $N_2 = 0$.

In steady state there is no net mass flux of polymer normal to the wall ($j = 0$), and the formal solution to (10) for the number density profile is

$$n(y) = n\left(\frac{h}{2}\right) exp\left[\int_{h/2}^{y} (L_d(z)\left(\frac{1}{z^2} - \frac{1}{(h-z)^2}\right) + \frac{V_{pp}}{D})dz\right], \quad (15)$$

where the local depletion length scale is

$$L_d(y) = \frac{K(y)}{D} = \frac{9}{16}\frac{N_1 - N_2}{nkT}a. \quad (16)$$

We used the half-value of the concentration to define the depletion layer thickness, giving

$$\int_{h/2}^{h-\delta^*} L_d(z)\left(\frac{1}{z^2} - \frac{1}{(h-z)^2}\right)dz = \ln(1/2) + \frac{V_p}{D}[y_p - \delta^*], \quad (17)$$

where δ^* is the depletion layer thickness predicted by the model. It is assumed that the depletion layer thickness is smaller than the interaction distance, so that $y_p > \delta^*$. Otherwise, the concentration is reduced to one half before the polymer interaction takes place, and the correction has no effect. For high Weissenberg numbers, we obtain the approximation [10]

$$\frac{\overline{L}_d}{\delta^*}\left[\frac{4\delta^*}{h} - \frac{\delta^*/h}{1-\delta^*/h} - 1\right] = \ln(2) + \frac{V_p}{D}[y_p - \delta^*] \equiv \ln(2) + \alpha - \beta\delta^*, \quad (18)$$

with a characteristic depletion length scale $\overline{L}_d$ that represents the typical value across the entire depletion layer in the absence of adsorption effects. By using asymptotic expansions for high Wi [31],

$$\overline{L}_d = \frac{9}{16}2^{1/3}a(bWi)^{2/3}. \quad (19)$$

We found an improved fit to the data when the polymer persistence length a diminished with Weissenberg number, as we found earlier in the absence of adsorption effects [10], and we use the same correction here. The parameter b is the ratio between potential and thermal energy,

$$b = HR_0^2/kT, \quad (20)$$

in terms of the FENE-P (finitely extensible non-elastic Peterlin) spring force parameter H, and the maximum spring extension R_0. For the coarse grained polymer chains, we adopt an average value $b = 1.5$ for the potential energy between two coarse grained DPD units.

To first order in δ^*/h, we obtain a solution to (18) of the form

$$\delta^* = \frac{\overline{L}_d^*}{1 + 4\overline{L}_d^*/h}, \quad (21)$$

where the corrected depletion length scale is

$$\overline{L}_d^* = \frac{\overline{L}_d}{\ln(2) - \alpha}, \quad (22)$$

which increases with increasing repulsion from the adsorbed layer. The corresponding Péclet number is

$$\alpha = \frac{V_p}{D}y_p = \frac{V_p}{D/y_p}. \quad (23)$$

The drift velocity V_p is necessarily proportional to the surface density of polymer as the net repulsion force on a flowing polymer is the sum of all forces acting on it, so that

$$V_p \simeq q\Gamma. \tag{24}$$

Hence, the Péclet number increases linearly with the adsorbed density as well, and q is a constant. A good fit to the adsorbed density from the simulations is obtained with the form

$$\Gamma = \Gamma_{max}\frac{Kc}{1+Kc} \times \left\{ \frac{1-f}{1+k(Wi)^r} + f \right\}, \tag{25}$$

where the first factor is the Langmuir isotherm, providing the zero-shear $Wi = 0$ limit. The factors K, k, r are fitted constants. Figure 8 (lower left) confirms that this algebraic functionality with Wi fits the adsorbed density well with an asymptote f for high Weissenberg number. A similar decrease with Wi was found by Dutta and co-workers using kinetic theory[15], although their results had $f = 0$.

The Péclet number can now be written

$$\begin{aligned} \alpha(Wi) &= q\frac{y_p}{D}\Gamma_{max}\frac{Kc}{1+Kc} \times \left\{ \frac{1-f}{1+k(Wi)^r} + f \right\} && (26) \\ &\equiv \frac{\alpha_{\max}}{1+k(Wi)^r} + \alpha_{\min}, && (27) \end{aligned}$$

where c is the bulk concentration for $Wi = 0$, and $\alpha_{\max}, \alpha_{\min}$ are functions of c and Γ_{max}. The Langmuir constant K corresponds to $Wi = 0$. The depletion layer thickness may decrease with higher shear rate as the adsorbed density decreases. However, this behavior depends on the rate of variation of the adsorbed density with Wi in relation to the variation of $\overline{L}_d \sim Wi^{2/3}a$. Indeed, the simulation results show that δ decreases with shear rate for the higher Wi (Figure 8, upper panels).

4.2. Adding non-dilute polymer-polymer interaction

In non-dilute solutions, polymer-polymer short range interaction may lead to increased back-diffusion towards the walls where the concentration gradient is large. Hence, the depletion layer tends to thin for increasing bulk concentration [32, 33, 23]. We introduce a corresponding drift velocity V_c,

$$j = V_d(y)n - D\partial_y n + V_{pp}(y)n + V_c(y)n. \tag{28}$$

The collisional drift is due to amplification of the diffusion coefficient and to first order, the associated increase in the mass flux is [34]

$$V_c(y)C = -k_D D C \partial_y C, \tag{29}$$

where $k_D C \ll 1$, and C is the local concentration in terms of mass fraction, and k_D is of order unity. Hence,

$$V_c(y) = -k_D D \partial_y C \simeq -k_D D \frac{C_b}{l}, \tag{30}$$

and V_c is sensitive to the local concentration gradient at the boundary of the depletion layer. Here, l is the length scale of the concentration gradient, and C_b is the bulk concentration measured as the average value within the depletion layers. This was fitted with $C_b = \zeta(1 - m\Gamma)$, where m and ζ are constants. The gradient length scale l could be found from the measured concentration gradient $\partial_y C$, by $l = C_b/(\partial_y C)$.

The final model of the Péclet number that includes both collisional and adsorbed layer effects, is then

$$\alpha(Wi) = \frac{\alpha_{\max}}{1 + k(Wi)^r} + \alpha_{\min} - \alpha_c \frac{C_b}{l}, \tag{31}$$

where α_c is constant. This was used together with (21) and (22) to model the depletion layer thickness.

4.3. Comparison to the simulations

The upper integration limit h of the integral (17) is by definition the position in the channel where the concentration of free-flowing polymer has declined to zero. This is at the boundary of the adsorbed layer in our case, and not at the solid wall. For the simulation data, we defined the depletion layer thickness with the solid wall as the reference point as discussed above. Thus, the depletion layer model is comparable to the data if the thickness of the adsorbed layer δ_{ads} is added to the model result,

$$\delta^* = \frac{\overline{L}_d^*}{1 + 4\overline{L}_d^*/h} + \delta_{\text{ads}}. \tag{32}$$

This model captures the trends and magnitudes in the simulation data, seen by comparison of the upper panels in Figure 8.

The average concentration gradient in the boundary of the depletion layer was taken from the measured concentration profiles. It was estimated as the difference between the maximum concentration in the bulk (for the two concentration peaks) and the minimum concentration in the depletion layer, divided by the distance between these two points. For the preadsorbed case, the concentration gradient was significantly higher for all Weissenberg numbers. The 5% and 10% cases had similar gradients (23.9 and 24.6 for $Wi = 4$, and 17.9 and 29.6 for $Wi = 8$, in normalized units). The 5% preadsorbed case had higher gradients (29.4 for $Wi = 4$, and 35.4 for $Wi = 8$).

The parameters $\alpha_{\max}$ and $\alpha_{\min}$ were found by fitting the adsorption model for Γ to the adsorbed density data. This implies that the history effects are incorporated as input parameters via the measured adsorbed density at high and low shear rates. A constant α_c, and varying l corresponding to the measured gradients, resulted in a good overall fit to the simulation data. The area fraction (Figure 8, lower left panel) was fitted with the function for $\Gamma(Wi)$ given above, and served as input to the model. The bulk concentration $C_b(Wi) \sim 1 - m\Gamma(Wi)$ increases significanty with Weissenberg number (lower right panel) when the adsorbed density is reduced (lower left panel), and it increases more for smaller channel width.

5. Discussion

The role of the adsorbed layer is important in the context of polymer flooding also in terms of reduced permeability [6]. If the wall coverage is large, such that the velocity is close to zero at the interface between the adsorbed layer and the flow, then it is reasonable to treat the adsorbed layer as a solid structure, and reduce the channel width (or permeability) accordingly. If the wall coverage is moderate, then the layer next to the wall may constitute a mix of moving water and slowly moving polymer, and the velocity approaches zero only at the solid wall. In this case, it would be more correct to keep the original pore size or channel width when calculating the effective viscosity.

When the Weissenberg number (shear rate) is increased, the adsorbed density is reduced in general. However, the adsorbed amount of polymers in equilibrium is not solely dependent on the Weissenberg number for a given bulk concentration, but rather on the initial level of adsorption before shear is applied. This relates directly to primary and secondary polymer injection, where a secondary injection is already subject to an adsorbed layer deposited

during the primary injection. Once adsorption has occurred, the shear forces needed to induce desorption to a given adsorbed density is greater than the shear rates that are necessary to limit the adsorbed density to the same level (from an initially clean surface)[11]. The phenomenological model can account for this by treating the adsorbed density at high shear as an input parameter, which indirectly reflects the preadsorbed value of the surface density.

Reduced cross-channel diffusivity by polymer stretching (anisotropic diffusivity, or Kirkwood-diffusivity) was not accounted for in the phenomenological model, and this would operate to some level whether we have adsorption or not. A stretched out polymer in a straight channel would have lower wall-normal diffusivity and longer cross-stream diffusion time. The position of the polymer with respect to the wall can therefore depend on the initial position of the polymer in the simulations. It is therefore essential to have a uniform polymer distribution as an initial condition to make the results less sensitive to the initial configuration of the system. For the current simulations, the polymer length was limited, hence the cross channel diffusion would be higher than for the typical HPAM length (if the polymers chains are not broken/degraded by shear). This would also imply a smoother concentration profile than for HPAM, and the depletion layer thickness defined in terms of the half-value of the average bulk concentration would possibly be marginally larger for smoother density profiles.

Every polymer bead in our DPD simulation had the same property, while real polymers usually have only a few active sites along the polymer chain that can efficiently adsorb to the surface. Real polymers would then possibly have longer loop segments extending into the flow as compared to our DPD polymers, with an effectively wider and more "fuzzy" adsorbed layer. It would be possible in future studies to have different bead types with different adsorbtion properties to study the effects of longer loops extending into the flow.

6. Conclusions

Dissipative Particle Dynamics (DPD) simulations were used to quantify the effect of polymer adsorption on the depletion layer and effective shear viscosity in microchannel Poseuille flow. The depletion layer thickness can increase due to adsorbed polymer via polymer-polymer repulsion, leading to reduced effective viscosity. Repulsion between HPAM polymers used for

polymer flooding in oil reservoirs occurs between a few active groups in the polymer molecule in low salinity water as a result of electrostatic repulsion between charged carboxylate groups. One would therefore expect that the same mechanism operates in these systems. We found that the repulsion effect increased the depletion layer thickness and reduced the effective viscosity ($\mu_e = h^2 G/(12U)$. The depletion layer expansion was counteracted to some degree by non-dilute enhancement of the diffusivity.

The adsorbed density followed a shear modified isotherm, with lower polymer adsorption for higher shear rate, thereby reducing the repulsion and the depletion layer thickness for higher Weissenberg numbers. This is in stark contrast to a case with no polymer adsorption, where the depletion layer thickness increases monotonically with the shear rate (as $Wi^{2/3}$ from the dumbbell model).

A phenomenological depletion layer model $\delta(Wi, h)$ was developed by modifying the Ma-Graham dumbell model with wall repulsion and diffusion correction for non-dilute solutions, including a shear modified adsorption isotherm. This model is purely algebraic, and can serve as as input to effective viscosity models $\mu_e(Wi, \delta/h)$, such as the one we developed earlier [10]. The phenomenological model for the depletion layer contains many parameters, but we hope that the model can serve as a fruitful starting point to construct applied models since all the model ingredients are physically based.

The net outcome for the effective viscosity depends on the delicate balance between increased repulsion from the adsorbed layer (lowering the effective viscosity by depletion layer expansion), increased bulk concentration (increasing the effective viscosity), and enhanced gradient diffusion (increasing the effective viscosity by shrinking the depletion layer). For secondary polymer injection, we expect higher adsorbed density for the same shear rates, as it is more difficult to desorb previously injected polymer. This history effect influences the effcetive viscosity via the coupling between the adsorbed density and the depletion layer thickness.

Acknowledgements R. Skartlien and T. A. Espås were funded by IFE (SIS-rheology project). T. L. Palmer was funded part time by IFE and mainly by the IOR centre of Norway via the Research Council of Norway, ConocoPhillips Skandinavia AS, DONG Energy AS Denmark, Eni Norge AS, ENGIE, Lundin Norway AS, Maersk Oil Norway AS, Statoil Petroleum AS, Wintershall Norge, Schlumberger Norge AS, and Halliburton. The parallel

code was developed earlier by G. Baardsen (funded by IFE) and T.L. Palmer. We used the freewares VisIt, TeXstudio and makebst.

[1] Jendrejack, R. M., Schwartz, D. C., de Pablo, J. J., Graham, M. D. (2004). The Journal of Chemical Physics, 120(5).

[2] Ma, H., Graham, M. D. (2005). Physics of Fluids, 17(8):083103. doi: http://dx.doi.org/10.1063/1.2011367.

[3] Fang, L., Hu, H., Larson, R. G. (2005). Journal of Rheology, 49(1).

[4] Hernandez-Ortiz, J. P., Ma, H., de Pablo, J. J., Graham, M. D. (2006). Physics of Fluids, 18(12):123101. doi: http://dx.doi.org/10.1063/1.2397571.

[5] Cuenca, A., Bodiguel, H. (2013). Phys. Rev. Lett., 110:108304. doi: 10.1103/PhysRevLett.110.108304.

[6] Stavland, A., Jonsbråten, H. C., Lohne, A., Moen, A., Giske, N. H. (2010). Society of Petroleum Engineers, 131103:1–15.

[7] Delshad, M., Kim, D. H., Magbagbeola, O. A., Huh, C., Pope, G. A., Tarahhom, F. (2008). Society of Petroleum Engineers, 113620:1–15. doi:doi:10.2118/113620-MS.

[8] Hatzignatiou, D. G., Norris, U. L., Stavland, A. (2013). Journal of Petroleum Science and Engineering, 108:137 – 150. ISSN 0920-4105. doi:http://dx.doi.org/10.1016/j.petrol.2013.01.001.

[9] Graham, M. D. (2011). Annual Review of Fluid Mechanics, 43(1):273–298. doi:10.1146/annurev-fluid-121108-145523.

[10] Palmer, T. L., Baardsen, G., Skartlien, R. (2017). Journal of Dispersion Science and Technology, 0(0):1–17. doi:10.1080/01932691.2017.1306784.

[11] Lee, J.-J., Fuller, G. G. (1985). Journal of Colloid and Interface Science, 103(2):569 – 577. ISSN 0021-9797. doi:https://doi.org/10.1016/0021-9797(85)90132-8.

[12] Al-Hashmi, A., Luckham, P. (2010). Colloids and Surfaces A: Physicochemical and Engineering Aspects, 358(1):142 – 148. ISSN 0927-7757. doi:https://doi.org/10.1016/j.colsurfa.2010.01.049.

[13] Sheng, J. J. (2011). Modern Chemical Enhanced Oil Recovery. Gulf Professional Publishing, Burlington, MA, USA, 1 edition.

[14] Stuart, M. A. C., Scheutjens, J. M. H. M., Fleer, G. J. (1980). Journal of Polymer Science: Polymer Physics Edition, 18(3):559–573. ISSN 1542-9385. doi:10.1002/pol.1980.180180315.

[15] Dutta, S., Dorfman, K., Kumar, S. (2013). Journal of Non-Newtonian Fluid Mechanics, 139(174905):1–8.

[16] Groot, R. D., Warren, P. B. (1997). J. Chem. Phys., 107:4423–4435.

[17] Hoogerbrugge, P. J., Koelman, J. M. V. A. (1992). Europhys. Lett., 19:155.

[18] Koelman, J. M. V. A., Hoogerbrugge, P. J. (1993). Europhys. Lett., 21:363–368.

[19] Kong, Y., Manke, C. W., Madden, W. G., Schlijper, A. G. (1994). Int. J. Thermophys., 15:1093–1101.

[20] Schlijper, A. G., Hoogerbrugge, P. J., Manke, C. W. (1995). J. Rheol., 39:567–579.

[21] Español, P., Warren, P. (1995). Europhys. Lett., 30:191–196.

[22] Symeonidis, V., Karniadakis, G. E., Caswell, B. (2006). The Journal of chemical physics, 125(18):184902.

[23] Millan, J. A., Laradji, M. (2009). Macromolecules, 42(3):803–810.

[24] Krafnick, R. C., García, A. E. (2015). The Journal of Chemical Physics, 143(24):243106.

[25] Pinches, M. R. R., Tildesley, D. J., Smith, W. (1991). Mol. Simul., 6:51–87.

[26] Sims, J. S., Martys, N. (2004). J. Res. Natl. Inst. Stand. Technol., 109:267–277.

[27] Revenga, M., Zuniga, I., Espanol, P., Pagonabarraga, I. (1998). International Journal of Modern Physics C, 09(08):1319–1328. doi: 10.1142/S0129183198001199.

[28] Liu, M., Meakin, P., Huang, H. (2007). Physics of Fluids, 19(3):033302. doi:http://dx.doi.org/10.1063/1.2717182.

[29] Finch, C. A. (1992). Polymer International, 28(3):256–256. ISSN 1097-0126. doi:10.1002/pi.4990280317.

[30] Bird, R., Dotson, P., Johnson, N. (1980). Journal of Non-Newtonian Fluid Mechanics, 7:213 – 235.

[31] Herrchen, M., Ottinger, H. (1997). Journal of Non-Newtonian Fluid Mechanics, 68:17 – 42.

[32] Chauveteau, G., Tirrell, M., Omari, A. (1984). Journal of Colloid and Interface Science, 100(1):41 – 54. ISSN 0021-9797. doi: http://dx.doi.org/10.1016/0021-9797(84)90410-7.

[33] Aragwal, U. S., Dutta, A., Mashelkar, R. A. (1994). Chemical Engineering Science, 49(11):1693–1717. ISSN 0009-2509. doi:10.1016/0009-2509(94)80057-X.

[34] Dutta, A., Mashelkar, R. (1984). Journal of Non-Newtonian Fluid Mechanics, 15(0):279–302.